Characterization of Functional Heme Domains from Soluble Guanylate Cyclase†

David S. Karow,‡ Duohai Pan,§,|| Joseph H. Davis,⊥ Sönke Behrends,# Richard A. Mathies,§,⊥ and Michael A. Marletta*,§,⊥,¶

Program in Cellular and Molecular Biology, University of Michigan, Ann Arbor, Michigan 48109, Departments of Chemistry and Molecular and Cell Biology, University of California, Berkeley, California 94720, Department of Pharmacology, University of Toronto, Toronto, Ontario, Canada M5S 1A8, and Division of Physical Biosciences, Lawrence Berkeley National Laboratory, Berkeley, California 94720

Received August 11, 2005; Revised Manuscript Received October 5, 2005

ABSTRACT: Soluble guanylate cyclase (sGC) is a heterodimeric, nitric oxide (NO)-sensing hemoprotein composed of two subunits, α1 and β1. NO binds to the heme cofactor in the β1 subunit, forming a five-coordinate NO complex that activates the enzyme several hundred-fold. In this paper, the heme domain has been localized to the N-terminal 194 residues of the β1 subunit. This fragment represents the smallest construct of the β1 subunit that retains the ligand-binding characteristics of the native enzyme, namely, tight affinity for NO and no observable binding of O_2. A functional heme domain from the rat β2 subunit has been localized to the first 217 amino acids β2(1−217). These proteins are ∼40% identical to the rat β1 heme domain and form five-coordinate, low-spin NO complexes and six-coordinate, low-spin CO complexes. Similar to sGC, these constructs have a weak Fe−His stretch [208 and 207 cm^{-1} for β1(1−194) and β2(1−217), respectively]. β2(1−217) forms a CO complex that is very similar to sGC and has a high ν_{CO} stretching frequency at 1994 cm^{-1}. The autoxidation rate of β1(1−194) was 0.073/min, while the β2(1−217) was substantially more stable in the ferrous form with an autoxidation rate of 0.003/min at 37 °C. This paper has identified and characterized the minimum functional ligand-binding heme domain derived from sGC, providing key details toward a comprehensive characterization.

Soluble guanylate cyclase (sGC)[1] is a well-characterized NO sensor, containing a heme-bound, N-terminal domain that binds NO, regulating a C-terminal guanylate cyclase. sGC catalyzes the conversion of GTP to cGMP, and it is a heterodimer, composed of α1 and β1 subunits. The ferrous heme is ligated to the β1 subunit via H105 (*1*), and when NO is bound, the activity of the enzyme is 300-fold elevated over basal activity (*2*). sGC has evolved to selectively bind NO and not O_2. It does not form a stable, isolable complex with O_2, permitting NO to bind selectively to the Fe^{2+} heme in an aerobic environment. This selectivity is essential for sGC to trap nanomolar concentrations of NO in the presence of a high competing concentration of O_2.

sGC has been characterized in eukaryotes ranging from *Drosophila* to humans, and until recently, there had been no reports of any other NO sensors except for sGC. Notably, no heme-containing NO sensors had been found in prokaryotes, which could be exposed to both exogenous and endogenous NO (*3*). However, a PSI-BLAST search using β1 (1−194) as the query sequence led to multiple hits in prokaryotic genomes (*4*, *5*). Two representative proteins were characterized, a 181 amino acid protein from *Vibrio cholerae* (VCA0720) and the heme domain from the *Thermoanaerobacter tengcongensis* Tar4 protein (*Tt*Tar4H) (*6*). VCA0720 is encoded in a histidine kinase-containing operon, while *Tt*Tar4H is fused to a methyl-accepting chemotaxis domain. These proteins share spectroscopic properties, sequence homology, and key conserved residues with the sGC heme domain and, therefore, were placed in the same family. Surprisingly, however, these proteins exhibited very different ligand-binding properties. For example, our spectroscopic data indicated that the predicted heme domain from *V. cholerae* had ligand-binding characteristics essentially identical to sGC, while *Tt*Tar4H was able to form a stable ferrous−oxy complex similar to the O_2-sensor *Ax*PDEA1 (*6*). Our results suggested that these sGC-like heme domains have evolved specific ligand-binding properties that allow them to function as sensors for NO or O_2, and therefore, we have named it the H−NOX (Heme−Nitric oxide/OXygen-binding) domain.

Previously, we had localized the heme-binding region of sGC to residues 1−385 of the β1 subunit (*1*, *7*). β1(1−385) includes a predicted coil−coil region and is isolated as a

† This work was supported in part by the LDRD Fund of the Lawrence Berkeley National Laboratory (M.A.M.) and by NIH grant EY-02051 (R.A.M.).

* To whom correspondence should be addressed: Department of Chemistry, University of California, Berkeley, CA 94720-1460. Telephone: 510-643-9325. Fax: 510-643-9388. E-mail: marletta@berkeley.edu.

‡ University of Michigan.

§ Department of Chemistry, University of California, Berkeley.

|| Present address: Pacific Northwest National Laboratory, K8-88 Richland, WA 99352.

⊥ Lawrence Berkeley National Laboratory.

University of Toronto.

¶ Department of Molecular and Cell Biology, University of California, Berkeley.

[1] Abbreviations: CO, carbon monoxide; sGC, soluble guanylate cyclase; NO, nitric oxide; *Tt*Tar4H, N-terminal 188 amino acids of *Thermoanaerobacter tengcongensis* Tar4 (heme domain); MCP, methyl-accepting chemotaxis protein; *Ax*PDEA1H, *Acetobacter xylinum* phosphodiesterase A1 heme domain; Mb, myoglobin; H−NOX domain, heme−nitric oxide/oxygen-binding domain.

10.1021/bi051601b CCC: $30.25
Published on Web 11/17/2005

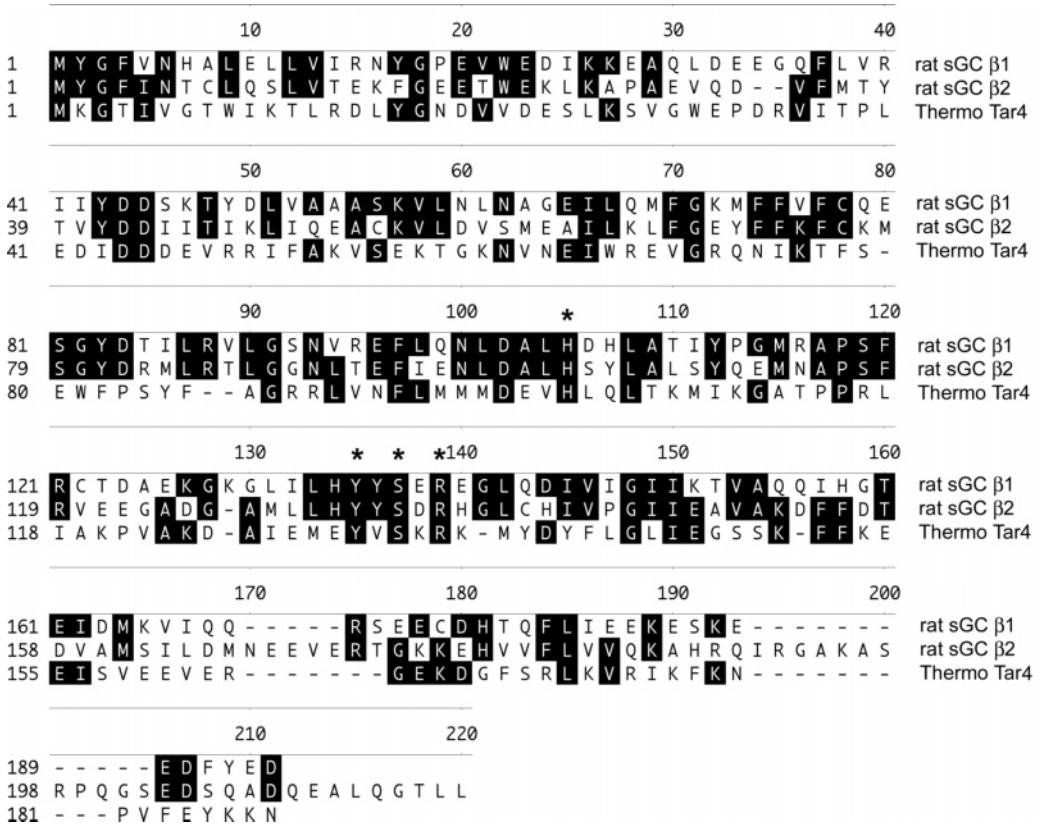

FIGURE 1: Alignment of rat β1(1−194) with rat β2(1−217) and the *T. tengcongensis* H−NOX domain. The alignment was generated using DNASTAR's Megalign program and the Clustal W algorithm. Conserved residues that are identical to the consensus sequence are shaded in black. Conserved residues discussed in the text are marked with an asterisk (His105, the heme ligand, and Tyr135, Ser137, and Arg139 using the rat β1 numbering).

homodimer although the associated spectral properties are essentially the same as those in the native enzyme. In an effort to determine the minimum sequence needed to retain the unique ligand-binding properties of the heme in sGC, we truncated and characterized several new constructs. In this paper, we show that the N-terminal 194 residues of the β1 subunit retains the unique ligand-binding properties of the full-length enzyme and appears to be the smallest functional β1 fragment. To further probe the selectivity of ligand binding in the sGC H−NOX domain, we have characterized this 194 amino acid β1 fragment representing the smallest sGC heme domain and the heme domain from the rat β2 subunit.

The β2 subunit is 43% identical to rat β1(1−194) (Figure 1) and was cloned from rat and kidney cDNA libraries (*8*−*10*). Its primary localization appears to be the kidney and liver (*8*). Unlike the β1 subunit, it contains an isoprenylation motif at its C terminus, which could lead to membrane localization (*8*). The functional relationship between the β1 and β2 subunits is not presently well-characterized. Because of their sequence similarity, it has been hypothesized that both subunits function to sense NO, but this has not been definitively demonstrated. Two recent papers have described NO-stimulated β2 cyclase activity in overexpressed cells, although the stimulation was much weaker compared to α1/β1 heterodimeric sGC (*10*, *11*). Thus, it appears that this subunit is a catalytically active NO-sensing homodimer, although no studies have been performed on purified protein. In this paper, we show that β2(1−217) is able to form a five-coordinate NO complex and is unable to form a stable $Fe^{2+}-O_2$ complex as observed for native sGC and the β1 subunit.

MATERIALS AND METHODS

Construction of Expression Plasmids. PCR (PfuTurbo, Stratagene) was used to amplify β1(1−194) and β2(1−217) from β1(1−385) and the full-length rat β2 clone (containing the additional N-terminal 60 amino acids) (*10*), respectively. The upstream primers were 5′-GGAATTCCATATGTACG-GTTTTGTGAACCATGCC-3′ and 5′-GGAATTCCATAT-GTATGGATTCATCAACACCTGC-3′ and the downstream primers were 5′-ATAGTTTAGCGGCCGCTCAATCTTCAT-AAAAATCCTCTTCTTTTG-3′ and 5′-ATAGTTTAGCG-GCCGCTCAAAGGAGTGTTCCCTGGAGAGCCTC-3′ for β1(1−194) and β2(1−217), respectively. Primers were obtained from Qiagen, except for the upstream primer for β2(1−217), which was obtained from GibcoBRL. Amplified PCR products were cloned into pET-20b (Novagen) and sequenced (UC Berkeley sequencing core and Elim Biopharmaceuticals, Inc.).

Protein Expression. Expressions were performed as described previously (*1*) with the following modifications. Plasmids were transformed into Tuner DE3 plysS cells (Novagen). Cultures were grown to an OD_{600} of 0.5−0.6 and cooled to 27 °C. IPTG (Promega) was added to 10 μM, and aminolevulinic acid was added to 1 mM. Cultures were grown overnight for 14−18 h and then harvested.

Protein Purification. β1(1−194) was purified in the following manner: frozen cell pellets from 3 L of culture were thawed quickly at 37 °C and resuspended in 120 mL

of buffer A [50 mM DEA at pH 8.5, 20 mM NaCl, 5 mM DTT, 1 mM Pefabloc (Pentapharm), and 5% glycerol]. Resuspended cells were lysed with sonication and, subsequently, with an Emulsiflex-C5 high-pressure homogenizer at 20 000 psi (Avestin, Inc.). Lysed cells were centrifuged at 100000*g* for 40 min. The supernatant was collected and reduced with ~500-fold excess dithionite, which was based on a final yield of 20 mg of pure protein. (Dithionite was used throughout the prep to keep the protein reduced because it oxidized over several hours and sometimes aggregated when oxidized. To minimize unwanted side effects of dithionite in aerobic conditions, we purged all of the chromatography buffers with nitrogen gas before use.) The supernatant was applied to a 50 mL (2.5 × 11 cm) Toyopearl SuperQ 650 M (Tosohaas) anion-exchange column at 2.5 mL/min. The column was washed with 2 column volumes of buffer A at 2.5 mL/min and eluted with a linear gradient of NaCl from 20 to 750 mM in a total volume of 340 mL at 3.5 mL/min. Fractions were selected on the basis of the intensity of the red/brown color. The eluate (50 mL) was concentrated to 4 mL using 15 mL of 10K MWCO spin concentrators (Millipore) and reduced with ~100-fold excess dithionite. The concentrated proteins were applied to a prepacked Superdex S75 HiLoad 26/60 gel-filtration column (Pharmacia) that had been equilibrated with TEA at pH 7.5, 50 mM NaCl, 5 mM DTT, and 5% glycerol. The flow rate was 1.5 mL/min. Fractions containing β1(1−194) were pooled, reduced with ~100-fold excess dithionite, and applied to a POROS HQ 7.9 mL (1 × 10 cm, 10 μm) anion-exchange column (Applied Biosystems) that had been equilibrated with buffer B (50 mM TEA at pH 7.5, 50 mM NaCl, 5 mM DTT, and 5% glycerol). The column was washed with 3 column volumes of buffer B at 10 mL/min and developed with a linear gradient of NaCl from 50 to 500 mM in a total volume of 140 mL at the same flow rate. β1(1−194)-containing fractions were pooled and stored at −70 °C.

β2(1−217) was purified as described above, except for the following modifications: dithionite was not added before each chromatographic step because it did not readily oxidize and aggregate. Buffer A contained 50 mM DEA at pH 8.5 and 25 mM NaCl, and the flow rate for loading in the first anion-exchange step was 1.5 mL/min. The supernatant was applied to a 100 mL (2.5 × 21 cm) Toyopearl DEAE 650M anion-exchange column (Tosohaas) and washed with 3 column volumes of buffer A. The column was developed with a linear NaCl gradient from 20 to 500 mM (800 mL), and the flow rate for loading, washing, and eluting was 1.2 mL/min. The high-resolution, anion-exchange step included 5 mM DTT.

UV/Vis Spectroscopy. All spectra were recorded in an anaerobic cuvette on a Cary 3E spectrophotometer equipped with a Neslab RTE-100 temperature controller set at 10 °C. Spectra were recorded from proteins in a solution of 50 mM TEA at pH 7.5 and 50 mM NaCl (buffer C). The heme concentration was ~7 μM. Protein samples were placed into the anaerobic cuvette in an anaerobic glovebag (Coy). Fe^{2+}-unligated protein samples were prepared in the following manner: purified protein was made anaerobic in an O_2-scavenged gas train with 10 cycles of alternate evacuation and purging with purified argon and brought into an anaerobic glovebag. Because β1(1−194) was susceptible to oxidation, it was first reduced anaerobically using dithionite (~100 equiv). The dithionite was then removed using a PD10 desalting column that had been equilibrated with buffer C. For consistency, β2(1−217) was prepared in the same manner. The CO complexes were generated by adding Fe^{2+}-unligated protein to a sealed Reacti-Vial (Pierce) that contained CO (Airgas). NO complexes were generated by preparing an anaerobic solution of diethylamine NONOate (Caymen) in buffer C (~10 mM) in a sealed Reacti-Vial. The headspace (1 mL) was then removed using a gastight syringe and delivered to an Fe^{2+}-unligated protein sample contained in a sealed Reacti-Vial.

Extinction Coefficient Determination. An anaerobic, Fe^{2+}-unligated, UV/vis spectrum was recorded for each protein sample. These samples, along with the Mb standard, were prepared anaerobically as described above with the following modification: bound O_2 was removed by ferricyanide oxidation (~100 equiv). The ferricyanide was then removed using a PD10 desalting column that had been equilibrated with buffer C, and then the protein was reduced using dithionite (~100 equiv). The dithionite was then removed in the same manner. For consistency, β1(1−194) and β2-(1−217) were prepared in the same way. The heme concentration was then determined for each sample by HPLC (*12*) and used to determine the Fe^{2+}-unligated extinction coefficient. This extinction coefficient was then used to determine the heme concentration and extinction coefficients for the CO and NO complexes from previously recorded UV/vis spectra. HPLC was used to determine the heme concentration using a protein C4 column (250 × 4.6 mm, 5 μm, Vydac) and a Hewlett−Packard Series II 1090 HPLC with a diode array detector. Each sample (25 μL) was applied to the C4 column that had been equilibrated with 0.1% trifluoroacetic acid (TFA). The column was developed with a linear gradient of 0−75% acetonitrile over 15 min followed by a linear gradient of 75−95% acetonitrile over 5 min. The flow rate was 1 mL/min.

Homology Modeling. Homology models of β1(1−194) and β2 (1−217) were generated using MODELLER following the methods described in ref *13*.

Resonance Raman Spectroscopy. Spectra of all samples were collected using a 413.1 nm laser excitation, except for the NO complexes, which were excited at 406.7 nm. A microspinning sample cell was used to minimize photoinduced degradation. Raman scattering was detected with a cooled, back-illuminated CCD (LN/CCD-1100/PB, Roper Scientific) controlled by a ST-133 controller coupled to a subtractive dispersion, double spectrograph (*14*). Raman spectra were corrected for wavelength dependence of the spectrometer efficiency by using a white lamp and calibrated with cyclohexane. The reported frequencies are accurate to ±2 cm^{-1}, and the resolution of the spectra is 8 cm^{-1}. All Raman spectra were obtained by subtracting the buffer background and baseline correction. The laser power at the sample was 3 mW, except for the CO complexes, where a power of 0.2 mW was used to avoid photolysis. Typical data acquisition times were 30 min.

All protein samples were placed into the Raman cell in an anaerobic glovebag. The heme concentration was 14 and 19 μM for β1(1−194) and β2(1−217), respectively. Protein samples for Raman spectroscopy were prepared as described above for UV/vis spectroscopy with the following modifica-

tions: ^{13}CO (99% containing ~10% $^{18}O_2$, Cambridge Isotopes) was prepared in a manner similar to the ^{12}CO complexes. ^{15}NO complexes were made in the following manner: A 1 mL solution of 0.5 M $K^{15}NO_2$ (Cambridge Isotopes) and a 1 mL solution of 1 M KI/H_2SO_4 were made anaerobic on an O_2-scavenged gas train and delivered into the anaerobic glovebag. The potassium nitrite solution (100 μL) was delivered to the KI solution using a gastight syringe. ^{15}NO-containing headspace (~1 mL) was then delivered to a protein sample contained in a sealed Reacti-Vial.

Oxidation Rates. Rat β1(1−194) and β2(1−217) (550 and 220 μM, respectively) were brought into an anaerobic chamber (Coy) and reduced at room temperature with sodium dithionite (20 mM final). Both proteins were then desalted using a PD-10 column and eluted in 50 mM triethanolamine and 50 mM NaCl. Each protein was then added to an anaerobic cuvette and removed from the chamber. Prior to acquiring the first spectra, each sample was diluted 5-fold with 50 mM triethanolamine and 50 mM NaCl that had been fully equilibrated with room air and the cuvette was then left open to atmospheric oxygen. Immediately (<10 s of dead time) after dilution with the aerobic buffer, spectra were acquired (β1, 1 scan/min for 100 min; β2, 1 scan/min for 60 min, 1 scan/10 min for 17 h) at 37 °C. Rate constants based on double difference plots (β1, Δ404 − Δ434; β2, Δ390 − Δ432) were then calculated and fit to single exponentials of the form $f(x) = A(1 - e^{-kx})$.

RESULTS

Cloning, Expression, and Purification. N-Terminal sGC β1 heme-binding region fragments were generated by subcloning specific constructs into the *Escherichia coli* expression vector pET-20b. The shortest region that was subcloned, had heme-bound, and expressed well was β1(1−194). For example, β1(1−189) was cloned, expressed, and purified, and relative to the longer constructs, it was poorly expressed and unstable. Therefore, β1(1−194) was the specific construct that was chosen for further studies.

For the β2 H−NOX domain, we initially attempted the expression of the full-length β2 subunit (*10*), and it was cloned into the bacterial expression vector pET-20b. After expression and purification, the results clearly showed that a soluble heme-bound protein was made but appeared to be truncated, as demonstrated by SDS−PAGE (data not shown). Mass spectral analysis yielded a heme-bound, N-terminal, 217 amino acid fragment, confirming that the protein was indeed truncated (data not shown). It appears that an endogenous *E. coli* protease cleaved this fragment from the full-length protein. The 5651 base pairs of the rat β2 subunit coding for residues 1−217 were then cloned into pET-20b and further characterized.

β1(1−194) and β2(1−217) were expressed in *E. coli* and purified as described in the Materials and Methods. These proteins were estimated to be >95% pure on the basis of Coomassie staining of samples resolved by SDS−PAGE (data not shown). Yields were ~5 and 13 mg/L of cell culture for β1(1−194) and β2(1−217), respectively. β2(1−217) was isolated in the Fe^{2+}-unligated state (Soret maximum ~ 431 nm). Dithionite was needed to keep β1(1−194) reduced throughout the purification, because it was found to oxidize readily (see the Materials and Methods). UV/vis and resonance Raman spectroscopy were then used to characterize the heme environment and ligand-binding characteristics of both proteins.

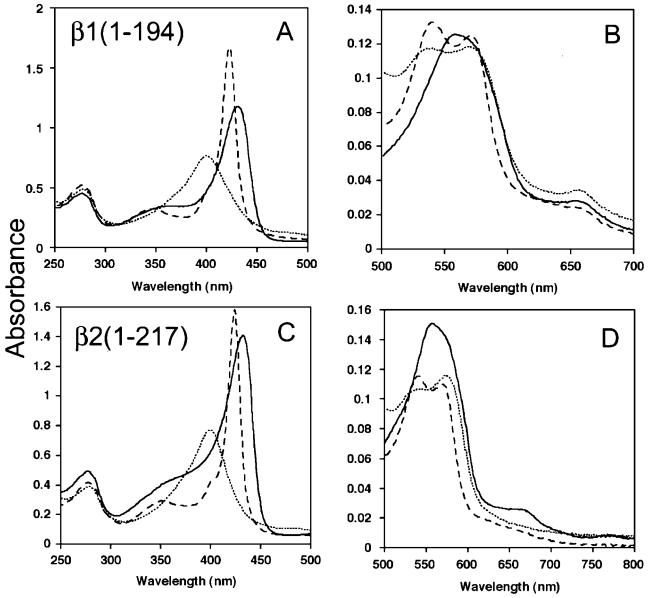

FIGURE 2: Electronic absorption spectra of β1(1−194) and β2(1−217) showing the Soret maximum and α/β region. Reduced, unligated (—); CO complex (- - -); and NO complex (···). The heme concentration was ~7 μM.

Table 1: UV−Vis Peak Positions[a] and Extinction Coefficients[b]

protein	Soret	β	α	ref
Fe^{2+}-unligated				
sGC	431 (111)	555 (14)		*2*
β1(1−194)	431 (166)	558 (17.7)		*c*
β2(1−217)	433 (155)	557 (17.1)		*c*
Hb	430 (133)	555 (12.5)		*15*
CO-bound				
sGC	423 (145)	541 (14)	567 (14)	*2*
β1(1−194)	423 (235)	541 (18.7)	571 (17.6)	*c*
β2(1−217)	424 (248)	541 (18.1)	570 (17.2)	*c*
Hb	419 (191)	540 (13.4)	569 (13.4)	*15*
NO-bound				
sGC	398 (79)	537 (12)	572 (12)	*2*
β1(1−194)	400 (108)	537 (16.5)	570 (16.7)	*c*
β2(1−217)	399 (121)	543 (16.8)	574 (18.1)	*c*
Hb	418 (130)	545 (12.6)	575 (13.0)	*15*

[a] Values in nm. [b] Values in mM^{-1} cm^{-1}. [c] This paper.

UV/vis Absorption Spectroscopy. UV/vis spectra are shown in Figure 2, and the data with extinction coefficients are summarized in Table 1 and compared to sGC (*2*) and hemoglobin (*15*). Details of the individual complexes are discussed where relevant below.

Fe^{2+}-Unligated and CO Complexes. These two β-subunit constructs have spectra that are similar to one another and to full-length sGC. The spectra of the Fe^{2+}-unligated hemes in both β-subunit constructs exhibit Soret bands at ~431 nm and a single broad α/β band at ~560 nm. The addition of CO to the anaerobically reduced proteins resulted in CO complexes with sharp Soret bands at ~424 nm, increases in the extinction coefficient, and observable α/β bands. The shape and absorption maxima of the Soret and α/β bands for both the Fe^{2+}-unligated and CO complexes are very similar to full-length sGC (*2*), suggesting that the reduced proteins are five-coordinate, high-spin and the CO complexes are six-coordinate, low-spin.

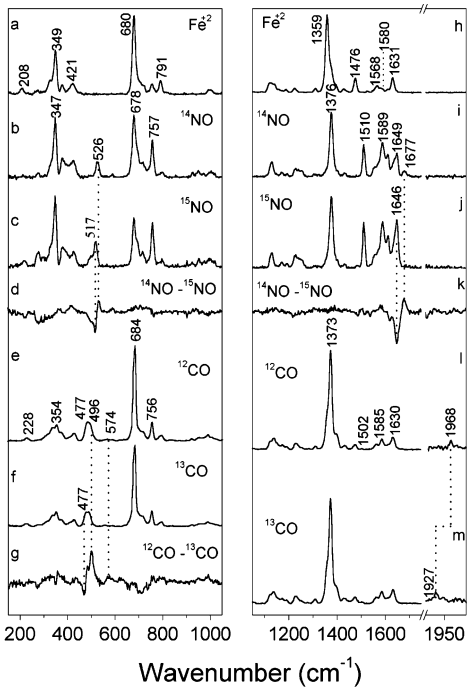

FIGURE 3: β1(1−194) resonance Raman spectra. Fe^{2+} unligated in the low- (a) and high- (h) frequency regions; ^{14}NO and ^{15}NO complexes and their difference spectra in the low- (b−d) and high- (i−k) frequency regions, respectively; ^{12}CO and ^{13}CO complexes and their difference spectra in the low- (e−g) and high- (l and m) frequency regions, respectively. The heme concentration was 14 μM. The Raman intensity was normalized to the ν_4 mode. The asterisks indicate subtraction artifacts.

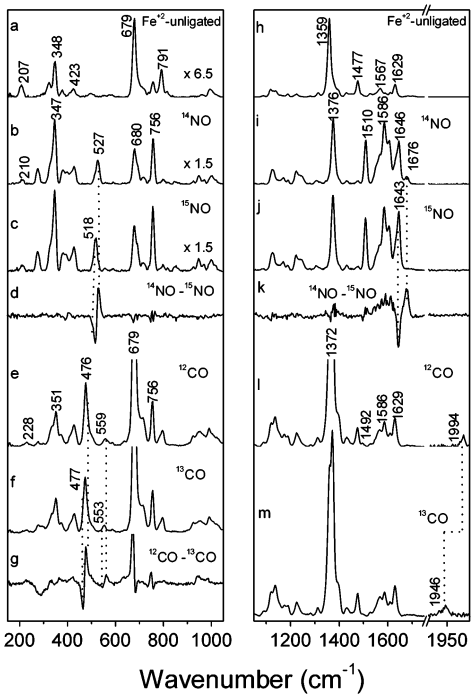

FIGURE 4: β2(1−217) resonance Raman spectra. Fe^{2+} unligated in the low- (a) and high- (h) frequency regions; ^{14}NO and ^{15}NO complexes and their difference spectra in the low- (b−d) and high- (i−k) frequency regions, respectively; ^{12}CO and ^{13}CO complexes and their difference spectra in the low- (e−g) and high- (l and m) frequency regions, respectively. The heme concentration was 19 μM. The Raman intensity was normalized to the ν_4 mode. The asterisks indicate subtraction artifacts.

NO Complexes. The NO complexes of β1(1−194) and β2-(1−217) are similar to those of full-length sGC, exhibiting broadened Soret bands at ∼399 nm, decreases in the extinction coefficient, and observable α/β bands. These spectra are identical to previously characterized five-coordinate, NO complexes (*2*).

Resonance Raman Spectroscopy. Raman spectra are shown in Figures 3 and 4 [β1(1−194) and β2(1−217), respectively], and the data are summarized in Tables 2, 3, and 4 (Fe^{2+} unligated, CO adducts, and NO adducts, respectively) along with comparisons to sGC (*16*, *17*), Mb (*18*−*23*), *Acetobacter xylinum* PDEA1H (the heme domain of *Ax*PDEA1) (*24*), rat sGC β1(1−385) (*25*), FixLN (the heme domain of FixL) (*26*), *Alcaligenes* xylosoxidans cyt c′ (*27*, *28*), HemAT-Bs (*29*), and CooA (*30*). Specific complexes are described below.

Fe^{2+}-Unligated Complexes. In the high-frequency region, the heme skeletal marker bands are observed. These include ν_4, which is sensitive to the oxidation state of the heme, and ν_3 and ν_2, which are sensitive to the spin and coordination state of the heme iron (*31*). The heme skeletal markers are similar to the corresponding bands in histidine-ligated, five-coordinate, high-spin, Fe^{2+} heme proteins such as sGC. In the low-frequency spectrum, bands at 208 and 207 cm^{-1} are observed for β1(1−194) and β2(1−217), respectively. These bands are assigned to the ν_{Fe-His} stretching mode, on the basis of previous observations that, in most histidine-ligated, Fe^{2+}−heme complexes, this stretching frequency is usually between 200 and 250 cm^{-1} (*32*) and that in the NO and CO adducts this band was absent. We conclude that, when reduced, these proteins contain a five-coordinate, high-spin heme.

Table 2: Heme Skeletal Vibrations and Vibrational Modes[a]: Fe^{+2}-Unligated Proteins

protein	cs[b]	ν_{10}	ν_2	ν_3	ν_4	Fe−His	ref
sGC	5	1606	1562	1471	1358	204	*16*, *17*
β1(1−385)	5	1607	1563	1474	1358	206	*25*
β1(1−194)	5	1608	1568	1476	1359	208	*c*
β2(1−217)	5	1609	1567	1477	1359	207	*c*
*Tt*Tar4H	5	1600	1575	1471	1354	218	*6*
Mb	5	1607	1563	1471	1357	220	*18*
HemAT-Bs	5	nr[d]	1558	1469	1352	225	*29*
*Ax*PDEA1H	5	1607	1557	1469	1354	212	*24*
*Ax*cyt c′	5	1603	1577	1469	1351	231	*27*

[a] Values in cm^{-1}. [b] Coordination state. [c] This paper. [d] Not reported.

Table 3: Heme Skeletal Vibrations and Vibrational Modes[a]: CO Complexes

protein	cs[b]	ν_{10}	ν_2	ν_3	ν_4	ν_{Fe-CO}	ν_{C-O}	δ[c]	ref
sGC	6	1629	1583	1500	1371	472[d]/487	1987	562	*16*, *17*
β1(1−385)	6	nd[e]	1582	1496	1373	478[d]/494	1987	564	*25*
β1(1−194)	6	1631	1586	1502	1375	477/496	1968	574	*f*
β2(1−217)	6	1629	1586	1493	1372	476	1994	559	*f*
*Tt*Tar4H	6	1620	1580	1496	1369	490	1989	567	*6*
Mb	6	1637	1587	1498	1372	512	1944	577	*21*
HemAT-Bs	6	nr[g]	1578	1495	1368	494	1964	nr	*29*
*Ax*PDEA1H	6	nr	nr	nr	nr	493	1973	581	*24*
*Ax*cyt c′	6	no[h]	1596	nr	1368	491	1966	572	*27*

[a] Values in cm^{-1}. [b] Coordination state. [c] Fe−C−O bending mode. [d] Represents the dominant frequency. [e] Not determined. [f] This paper. [g] Not reported. [h] Not observed.

CO Complexes. The heme skeletal markers in the high-frequency region are similar to the corresponding bands from histidine-ligated, six-coordinate, low-spin, Fe^{2+} heme proteins such as sGC. In the low-frequency spectrum, isotope-

Table 4: Heme Skeletal Vibrations and Vibrational Modes[a]: NO Complexes

protein	cs[b]	ν_{10}	ν_2	ν_3	ν_4	ν_{Fe-NO}	ν_{N-O}	ref
sGC	5	1646	1584	1509	1375	525	1677	*16, 17*
β1(1−194)	5	1647	1586	1510	1376	526	1677	*c*
β1(1−385)	5	1646	1585	1509	1376	526	1676	*25*
β2(1−217)	5	1646	1586	1510	1376	527	1676	*c*
*Tt*Tar4H	6	1625	1580	1496	1370	553	1655	*6*
Mb	6	1638	1584	1501	1375	554	1624	*19, 20*
*Ax*cyt c′	5	1641	1592	1506	1373	526	1661	*27*
*Ax*cyt c′	6	1638	1596	1504	nr[d]	579	1624	*28*
FixLN (20 °C)	6	1632	nr	1498	nr	558	no[e]	*26*
FixLN (20 °C)	5	1646	nr	1509	nr	525	1676	*26*
*Ax*PDEA1H	6	nr	nr	nr	nr	560	1637	*24*
Mb(H64V)	6	nr	nr	nr	nr	557	1640	*22*
Mb(H93G)	5	nr	nr	nr	nr	535	1670	*22*
Mb(H64V/H93G)	5	nr	nr	nr	nr	534	1684	*22*
CooA	5	nr	nr	nr	nr	523	1672	*30*
Mb H93Y	5	nr	nr	nr	nr	524	1672	*23*

[a] Values in cm^{-1}. [b] Coordination state. [c] This paper. [d] Not reported. [e] Not observed.

sensitive bands are observed at 477 and 496 cm^{-1} for β1-(1−194) and 476 cm^{-1} for β2(1−217). These bands are assigned to the ν_{Fe-CO} stretching mode on the basis of their isotopic shift and their similarity to the ν_{Fe-CO} frequency for full-length sGC (472/487 cm^{-1}) and other six-coordinate, low-spin heme proteins (Table 2). The two ν_{Fe-CO} frequencies in full-length sGC are likely due to different Fe−CO conformations (*25*), and this may also account for the two ν_{Fe-CO} frequencies in β1(1−194). In the high-frequency spectrum, isotope-sensitive bands are observed at 1968 and 1994 cm^{-1} for β1(1−194) and β2(1−217), respectively. These bands are assigned to the ν_{CO} stretching mode on the basis of their isotopic shift and their similarity to the ν_{CO} frequencies of sGC (1987 cm^{-1}) and HemAT-Bs (1964 cm^{-1}) (Table 2). Similar to sGC, β2(1−217) has a high ν_{CO} stretching frequency. Therefore, β2(1−217) forms a CO complex that is the most similar to sGC. These complexes are six-coordinate, low-spin and are notable for their high ν_{CO} stretching frequency. CO-β1(1−194) is also six-coordinate, low-spin, like sGC, but its ν_{CO} frequency is closer to that of proteins with lower values, like HemAT-Bs (1964 cm^{-1}).

NO Complexes. For β1(1−194) and β2(1−217), the high-frequency spectra exhibit heme skeletal marker bands that are similar to the corresponding bands in five-coordinate NO−sGC. In the low-frequency spectra, isotope-sensitive bands are observed at 526 and 527 cm^{-1} for β1(1−194) and β2(1−217), respectively. These bands are assigned to the ν_{Fe-NO} stretching mode based on their isotopic shift and similarity to the ν_{Fe-NO} frequency in sGC (525 cm^{-1}). Isotope-sensitive bands are also observed in the high-frequency spectra [1676 and 1677 cm^{-1} for β2(1−217) and β1(1−194), respectively]. On the basis of their isotopic shift and similarity to the ν_{NO} frequency in sGC (1677 cm^{-1}), these bands are assigned to the ν_{NO} stretching mode. These data indicate that the NO complexes of β1(1−194) and β2(1−217) are five-coordinate and similar to sGC.

Oxidation Rates. Rat β1(1−194) was found to oxidize very quickly compared to full-length sGC, which is very stable to oxidation (Figure 5). When averaged over three experiments, the autoxidation rate of β1(1−194) was 0.073 min^{-1}. Rat β2(1−217) was substantially more stable in the ferrous form with an autoxidation rate of 0.003 min^{-1} at 37 °C. It should be noted that, while β1 appears to cleanly convert from a five-coordinate, high-spin Fe^{2+} complex (Soret λ_{max} at 431 nm) to a five-coordinate, high-spin Fe^{3+} complex (Soret maximum at 390 nm), the β2 oxidation is more complex. The high-spin, ferrous unligated (Soret λ_{max} at 432 nm) protein appears to oxidize to a mixture of high- and low-spin ferric complexes (Soret λ_{max} at 393 and 415, respectively). To support this conclusion, after oxidation with potassium $(Fe(CN)_6)^{3-}$, the protein first forms a high-spin complex (Soret λ_{max} at 393 nm), which then converts to a mixture of high- and low-spin complexes (broad Soret λ_{max} at 415 nm) (data not shown).

DISCUSSION

The essential feature of sGC is the use of a ferrous heme with histidyl ligation to trap low concentrations of NO in the presence of a much higher O_2 concentration. The heme in sGC shows no measurable affinity for O_2, hence there is no competition for NO against a severe concentration gradient. The molecular basis for this remarkable ligand discrimination against O_2 has not been clear until recent findings indicated that sGC-like heme domains are present in prokaryotes. Characterization of these proteins has provided a molecular basis for this ligand discrimination (*5*, *6*, *33*). Because some members of the family form a stable complex with O_2, we have named the family H−NOX (Heme−Nitric oxide/OXygen) to more fully describe the family in terms of its ligand-binding properties.

Prior to the discovery of the H−NOX family, the strategy to characterize the sGC heme was focused on truncations of the β1 subunit in an effort to identify a stable heme domain fragment. These studies had identified a 385 amino acid fragment of the β1 subunit that retained the unique ligand-binding properties of native sGC (*1*, *7*). However, all attempts to crystallize this fragment failed, and we surmised that this failure was due to the tendency of this protein to form an unnatural homodimer. On the basis of this, constructs were designed to determine the minimum size of the β1 fragment that retained the native ligand-binding properties. Several constructs were generated and characterized; the smallest was a 194 amino acid fragment. Any construct smaller than this (1−189, for example) could not be isolated with a full equivalent of heme and gave low yields upon purification, suggesting that ∼190 amino acids is the minimum fragment for a stable heme domain.

β1(1−194) was examined further as reported here, but perhaps more importantly, this fragment served as a query sequence for genome searching that led us to the H−NOX family. In two recent papers, we have described two of these H−NOXs. The first protein was a 181 amino acid protein from *V. cholerae* (VCA0720), and the other was a 188 amino acid heme domain fragment from the *T. tengcongensis* Tar4 protein (*Tt*Tar4H) (*6*). The heme domain from *V. cholerae* has ligand-binding properties like that of sGC; namely, the ferrous protein does not form an O_2 complex but does form stable complexes with NO and CO. The *T. tengcongensis* heme domain on the other hand forms a very stable ferrous O_2 complex and like the globins will also form a CO and NO complex. We have also determined the crystal structure

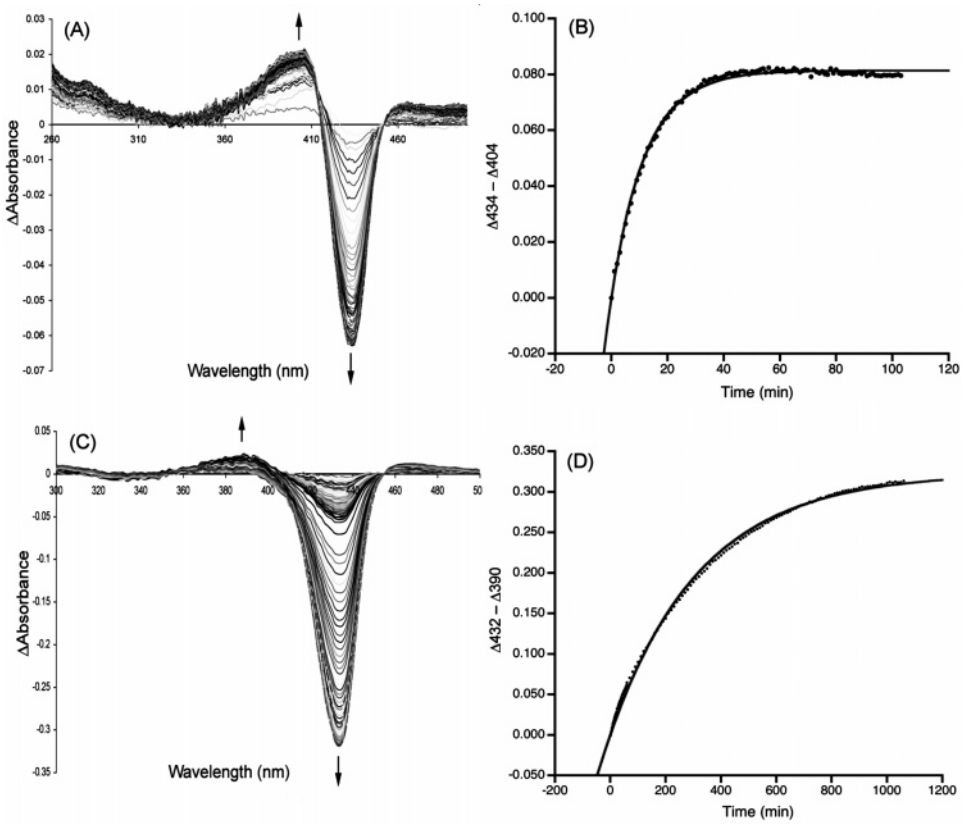

FIGURE 5: Autoxidation rates of β1(1−194) and β2(1−217). Shown in A are difference spectra associated with the autoxidation of β1-(1−194), and B shows a plot of the Δ434 − Δ404 versus time and a fit (gray line) to the data from which a rate constant was derived. C shows the difference spectra for the autoxidation of β2(1−217), and D shows a plot of Δ432 − Δ390 versus time and a fit to those data (gray line).

of the heme domain from *T. tengcongensis* which, as mentioned above, provided a molecular explanation for the discrimination against O_2 in the sGC-like proteins (*5*, *33*). In fact, on the basis of the structure of the *T. tengcongensis* H−NOX, we have recently converted β1(1−385) into a protein that now forms a stable $Fe^{2+}-O_2$ complex (*33*).

Although the β1(1−194) construct is the smallest fragment that was stable enough to characterize, it is clear that it is not as stable as sGC. The rate of oxidation to Fe^{3+} is very slow in sGC and, as shown in Figure 5, occurs much more quickly in β1(1−194). The Fe^{2+}-unliganded, $Fe^{2+}-NO$, and $Fe^{2+}-CO$ complexes are all identical to sGC; however, once the Fe^{2+}-unliganded complex is exposed to air, oxidation occurs. A $Fe^{2+}-O_2$ complex is not observed during oxidation, and the molecular steps involved in the oxidation are unknown. β2(1−217) on the other hand is much more stable (Figure 5) and more comparable to sGC and the previously characterized β1(1−385) in this respect. β2(1−217) is 43% identical to the β1 subunit and shares the key spectroscopic properties of sGC. Specifically, the Fe^{2+}-unligated forms of these proteins are five-coordinate, high-spin, and the CO complexes are six-coordinate, low-spin.

Moreover, similar to sGC, both β1(1−194) and β2(1−217) form a CO complex with unusually high ν_{CO} and low ν_{Fe-CO} stretching frequencies. sGC has one of the highest reported ν_{CO} stretching frequencies, and on the basis of this observation, it was previously suggested that the distal pocket of sGC has significant negative polarity (*34*). This is based on the observation that the ν_{CO} and ν_{Fe-CO} frequencies are inversely correlated and are sensitive to distal pocket polarity (*35*, *36*). Negative polarity in the distal pocket can inhibit Fe $d_\pi \rightarrow$ CO π^* back-bonding, weakening the Fe−CO bond order and strengthening the C−O bond order. However, a homology model of β1(1−194) and β2(1−217) based on the structure of the *Tt*Tar4H H−NOX shows no significant region of negative polarity that is close to the bound ligand. Figure 6 shows this model when viewed from below the heme and looking up into the distal pocket. Tyr140 is clearly visible in the *T. tengcongensis* H−NOX distal site, but there is no hydrogen-bonding donor or residue that would provide negative polarity in either model of β1(1−194) or β2(1−217), suggesting that the negative polarity hypothesis may not be correct. A ν_{Fe-CO}/ν_{CO} correlation, which was generated from model porphyrin and hemoprotein frequencies, is shown in Figure 7. The closest ν_{CO} and ν_{Fe-CO} frequencies to sGC are from a Mb mutant (H64V/V68T), which increases negative polarity in the distal pocket (*37*). The high ν_{C-O} and low ν_{Fe-CO} stretching frequencies observed in β1(1−194) and β2(1−217), while consistent with distal pockets containing negative polarity, would seem to be dependent upon other factors.

β1(1−194) has higher ν_{Fe-CO} and lower ν_{CO} frequencies compared to sGC. For example, the ν_{CO} frequency is observed at 1968 cm^{-1} compared to 1987 cm^{-1} for sGC. Moreover, a broad band with two peaks of roughly equal intensity at 477 and 496 cm^{-1} were observed for the ν_{Fe-CO} stretching frequencies. Two frequencies were also observed for sGC and for the previously characterized heme-binding region β1(1−385) (*25*): an intense band at 472 cm^{-1} and a very weak shoulder at 487 cm^{-1} for sGC and an intense band

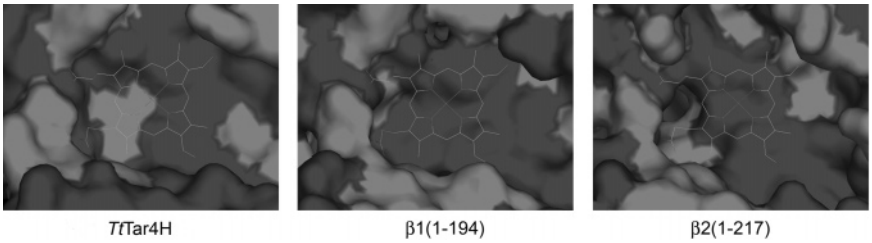

FIGURE 6: Homology models of the distal pockets. Homology models of the β1 and β2 were generated using MODELLER following the methods described in ref *13*. The view in the model is from below the heme and looking up into the distal pocket. Hydrogen-bonding donors or residues that would provide negative polarity are shown in light gray. Tyr140 in the *Tt*Tar4H distal site is clearly visible; however, there is none visible in either model of β1(1−194) or β2(1−217).

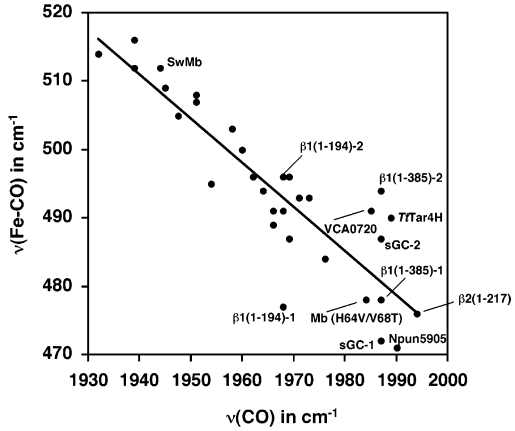

FIGURE 7: ν_{Fe-CO}/ν_{CO} correlation for six-coordinate CO adducts of model porphyrins and hemoproteins. Values for the metalloporphyrins and hemoproteins were obtained from Kerr et al., Table 2, complexes 1−15 (*38*); Table 3 in this paper; CooA (*39*, *40*); *Ec*DosH (*24*); *Bj*FixL (*24*); Heme oxygenase (*41*, *42*); Sperm whale (Sw) Mb (*21*); and Mb (H64V/V68T) (*37*). For sGC, β1(1−385) and β1(1−194), the numeric suffix refers to the CO conformation with the low and high ν_{Fe-CO} frequency (1 and 2, respectively).

at 478 cm^{-1} and a weaker shoulder at 494 cm^{-1} for β1(1−385). Although the two bands observed in sGC and β1(1−385) have been attributed to different CO conformations, no definitive results have emerged to support this hypothesis.

β2(1−217) is very similar to the heme domain of sGC in that it is unable to form a stable $Fe^{2+}-O_2$ complex but does form a five-coordinate complex with NO. If we assume that the ligand-binding characteristics of β2(1−217) are representative of the full-length subunit, an assumption that is consistent with reduced β1(1−194) being spectrally similar to full-length sGC, then it is likely that the β2 subunit also senses NO. These results are consistent with two papers that show NO-sensitive guanylate cyclase activity in β2-expressing cells. The first showed NO-stimulated activity in rat β2-expressing SF9 cell lysates (*10*), and the second showed NO-stimulated activity in rat β2-expressing COS 7 cell lysates (*11*). Although the enzyme was not purified, the conclusion was that homodimeric β2 was the active protein. This would be the first example of a sGC that contained two heme cofactors per dimer and raises interesting questions regarding heme occupancy and regulation.

In summary, this paper has identified and characterized the minimum functional ligand-binding heme domain derived from sGC. This 194 amino acid N-terminal fragment was then used to identify prokaryotic homologues of predicted hemoprotein sensor domains that probably function as NO sensors in some organisms and O_2 sensors in others. In addition, the ligand-binding properties of a heme domain derived from the β2 subunit are reported. These results and others on this broadening family of proteins are providing key details toward a comprehensive characterization.

ACKNOWLEDGMENT

We thank Chinmay Majmudar for help with the initial characterization of β1(1−194) and Dr. Elizabeth Boon for critical input.

REFERENCES

1. Zhao, Y., and Marletta, M. A. (1997) Localization of the heme binding region of soluble guanylate cyclase, *Biochemistry 36*, 15959−15964.
2. Stone, J. R., and Marletta, M. A. (1994) Soluble guanylate cyclase from bovine lung: Activation with nitric oxide and carbon monoxide and spectral characterization of the ferrous and ferric states, *Biochemistry 33*, 5636−5640.
3. Watmough, N. J., Butland, G., Cheesman, M. R., Moir, J. W., Richardson, D. J., and Spiro, S. (1999) Nitric oxide in bacteria: Synthesis and consumption, *Biochim. Biophys. Acta 1411*, 456−474.
4. Iyer, L. M., Anantharaman, V., and Aravind, L. (2003) Ancient conserved domains shared by animal soluble guanylyl cyclases and bacterial signaling proteins, *BMC Genomics 6*, 490−497.
5. Pellicena, P., Karow, D. S., Boon, E. M., Marletta, M. A., and Kuriyan, J. (2004) Crystal structure of an oxygen binding H−NOX domain related to soluble guanylate cyclases, *Proc. Natl. Acad. Sci. U.S.A. 101*, 12854−12859.
6. Karow, D. S., Pan, D., Tran, R., Pellicena, P., Presley, A., Mathies, R. A., and Marletta, M. A. (2004) Spectroscopic characterization of the sGC-like heme domains from *Vibrio cholerae* and *Thermoanaerobacter tengcongensis*, *Biochemistry 43*, 10203−10211.
7. Zhao, Y., Schelvis, J. P., Babcock, G. T., and Marletta, M. A. (1998) Identification of histidine 105 in the β1 subunit of soluble guanylate cyclase as the heme proximal ligand, *Biochemistry 37*, 4502−4509.
8. Yuen, P. S. T., Potter, L. R., and Garbers, D. L. (1990) A new form of guanylyl cyclase is preferentially expressed in rat kidney, *Biochemistry 29*, 10872−10878.
9. Behrends, S., and Vehse, K. (2000) The β2 subunit of soluble guanylyl cyclase contains a human-specific frameshift and is expressed in gastric carcinoma, *Biochem. Biophys. Res. Commun. 27*1, 64−69.
10. Koglin, M., Vehse, K., Budaeus, L., Scholz, H., and Behrends, S. (2001) Nitric oxide activates the β2 subunit of soluble guanylyl cyclase in the absence of a second subunit, *J. Biol. Chem. 276*, 30737−30743.
11. Gibb, B. J., Wykes, V., and Garthwaite, J. (2003) Properties of NO-activated guanylyl cyclases expressed in cells, *Br. J. Pharmacol. 139*, 1032−1040.
12. Brandish, P. E., Buechler, W., and Marletta, M. A. (1998) Regeneration of the ferrous heme of soluble guanylate cyclase from the nitric oxide complex: Acceleration by thiols and oxyhemoglobin, *Biochemistry 37*, 16898−16907.
13. Fiser, A., and Sali, A. (2003) Modeller: Generation and refinement of homology-based protein structure models, *Methods Enzymol. 374*, 461−491.

14. Pan, D., Ganim, Z., Kim, J. E., Verhoeven, M. A., Lugtenburg, J., and Mathies, R. A. (2002) Time-resolved resonance Raman analysis of chromophore structural changes in the formation and decay of rhodopsin's BSI intermediate, *J. Am. Chem. Soc. 124*, 4857−4864.
15. Di Iorio, E. E. (1981) Preparation of derivatives of ferrous and ferric hemoglobin, in *Hemoglobins* (Antonini, E., Rossi-Bernardi, L., and Chiancone, E., Eds.) pp 57−71, Academic Press, New York.
16. Deinum, G., Stone, J. R., Babcock, G. T., and Marletta, M. A. (1996) Binding of nitric oxide and carbon monoxide to soluble guanylate cyclase as observed with resonance Raman spectroscopy, *Biochemistry 35*, 1540−1547.
17. Tomita, T., Ogura, T., Tsuyama, S., Imai, Y., and Kitigawa, T. (1997) Effects of GTP on bound nitric oxide of soluble guanylate cyclase probed by resonance Raman spectroscopy, *Biochemistry 36*, 10155−10160.
18. Choi, S., Spiro, T. G., Langry, K. C., Smith, K. M., Budd, D. L., and La Mar, G. N. (1982) Structural correlations and vinyl influences in resonance Raman spectra of protoheme comlexes and proteins, *J. Am. Chem. Soc. 104*, 4345−4351.
19. Tsubaki, M., and Yu, N. T. (1982) Resonance Raman investigation of nitric oxide bonding in nitrosylhemoglobin A and -myoglobin: Detection of bound N−O stretching and Fe−NO stretching vibrations from the hexacoordinated NO−heme complex, *Biochemistry 21*, 1140−1144.
20. Hu, S., and Kincaid, J. R. (1991) Resonance Raman spectra of the nitric oxide adducts of ferrous cytochrome P450cam in the presence of various substrates, *J. Am. Chem. Soc. 113*, 9760−9766.
21. Tsubaki, M., Srivastava, R. B., and Yu, N. T. (1982) Resonance Raman investigation of carbon monoxide bonding in (carbon monoxy)hemoglobin and -myoglobin: Detection of Fe−CO stretching and Fe−C−O bending vibrations and influence of the quaternary structure change, *Biochemistry 21*, 1132−1140.
22. Thomas, M. R., Brown, D., Franzen, S., and Boxer, S. G. (2001) FTIR and resonance Raman studies of nitric oxide binding to H93G cavity mutants of myoglobin, *Biochemistry 40*, 15047−15056.
23. Vogel, K. M., Hu, S., Spiro, T. G., Dierks, E. A., Yu, A. E., and Burstyn, J. N. (1999) Variable forms of soluble guanylyl cyclase: Protein−ligand interactions and the issue of activation by carbon monoxide, *J. Biol. Inorg. Chem. 4*, 804−813.
24. Tomita, T., Gonzalez, G., Chang, A. L., Ikeda-Saito, M., and Gilles-Gonzalez, M. A. (2002) A comparative resonance Raman analysis of heme-binding PAS domains: Heme iron coordination structures of the BjFixL, AxPDEA1, EcDos, and MtDos proteins, *Biochemistry 41*, 4819−4826.
25. Schelvis, J. P., Zhao, Y., Marletta, M. A., and Babcock, G. T. (1998) Resonance Raman characterization of the heme domain of soluble guanylate cyclase, *Biochemistry* 37, 16289−16297.
26. Lukat-Rodgers, G. S., and Rodgers, K. R. (1997) Characterization of ferrous FixL-nitric oxide adducts by resonance Raman spectroscopy, *Biochemistry 36*, 4178−4187.
27. Andrew, C. R., Green, E. L., Lawson, D. M., and Eady, R. R. (2001) Resonance Raman studies of cytochrome *c*′ support the binding of NO and CO to opposite sides of the heme: Implications for ligand discrimination in heme-based sensors, *Biochemistry 40*, 4115−4122.
28. Andrew, C. R., George, S. J., Lawson, D. M., and Eady, R. R. (2002) Six- to five-coordinate heme−nitrosyl conversion in cytochrome *c*′ and its relevance to guanylate cyclase, *Biochemistry 41*, 2353−2360.
29. Aono, S., Kato, T., Matsuki, M., Nakajima, H., Ohta, T., Uchida, T., and Kitagawa, T. (2002) Resonance Raman and ligand binding studies of the oxygen-sensing signal transducer protein HemAT from *Bacillus subtilis*, *J. Biol. Chem. 277*, 13528−13538.
30. Reynolds, M. F., Parks, R. B., Burstyn, J. N., Shelver, D., Thorsteinsson, M. V., Kerby, R. L., Roberts, G. P., Vogel, K. M., and Spiro, T. G. (2000) Electronic absorption, EPR, and resonance Raman spectroscopy of CooA, a CO-sensing transcription activator from *R. rubrum*, reveals a five-coordinate NO−heme, *Biochemistry 39*, 388−396.
31. Spiro, T. G., and Li, X.-Y. (1988) Resonance Raman spectroscopy of metalloporphyrins, in *Biological Applications of Raman Spectroscopy* (Spiro, T. G., Ed.) pp 1−37, John Wiley and Sons, New York.
32. Kitagawa, T. (1988) Heme protein structure and the iron−histidine stretching mode, in *Biological Applications of Raman Spectroscopy* (Spiro, T. G., Ed.) pp 97−131, John Wiley and Sons, New York.
33. Boon, E. M., Huang, S. H., and Marletta, M. A. (2005) A molecular basis for NO selectivity in soluble guanylate cyclase, *Nat. Chem. Biol. 1*, 53−59.
34. Kim, S., Deinum, G., Gardner, M. T., Marletta, M. A., and Babcock, G. T. (1996) Distal pocket polarity in the unusual ligand binding site of soluble guanylate cyclase: Implications for control of •NO binding, *J. Am. Chem. Soc. 118*, 8769−8770.
35. Cameron, A. D., Smerdon, S. J., Wilkinson, A. J., Habash, J., Helliwell, J. R., Li, T., and Olson, J. S. (1993) Distal pocket polarity in ligand binding to myoglobin: Deoxy and carbonmonoxy forms of a threonine68(E11) mutant investigated by X-ray crystallography and infrared spectroscopy, *Biochemistry 32*, 13061−13070.
36. Li, T., Quillin, M. L., Phillips, G. N., Jr., and Olson, J. S. (1994) Structural determinants of the stretching frequency of CO bound to myoglobin, *Biochemistry 33*, 1433−1446.
37. Biram, D., Garratt, C. J., and Hester, R. E. (1991) in *Spectroscopy of Biological Molecules* (Hester, R. E., and Girling, R. B., Eds.) pp 433−434, Royal Society of Chemistry, Cambridge, U.K.
38. Yu, N., and Kerr, E. A. (1988) Vibrational modes of coordinated CO, CN^-, O_2, and NO, in *Biological Applications of Raman Spectroscopy* (Spiro, T. G., Ed.) pp 39−96, John Wiley and Sons, New York.
39. Uchida, T., Ishikawa, H., Takahashi, S., Ishimori, K., Morishima, I., Ohkubo, K., Nakajima, H., and Aono, S. (1998) Heme environmental structure of CooA is modulated by the target DNA binding. Evidence from resonance Raman spectroscopy and CO rebinding kinetics, *J. Biol. Chem. 273*, 19988−19992.
40. Uchida, T., Ishikawa, H., Ishimori, K., Morishima, I., Nakajima, H., Aono, S., Mizutani, Y., and Kitagawa, T. (2000) Identification of histidine 77 as the axial heme ligand of carbonmonoxy CooA by picosecond time-resolved resonance Raman spectroscopy, *Biochemistry 39*, 12747−12752.
41. Takahashi, S., Ishikawa, K., Takeuchi, N., Ikeda-Saito, M., Yoshida, T., and Rousseau, D. L. (1995) Oxygen-bound heme−heme oxygenase complex: Evidence for a highly bent structure of the coordinated oxygen, *J. Am. Chem. Soc. 117*, 6002−6006.
42. Takahashi, S., Wang, J., Rousseau, D. L., Ishikawa, K., Yoshida, T., Takeuchi, N., and Ikeda-Saito, M. (1994) Heme-heme oxygenase complex: Structure and properties of the catalytic site from resonance Raman scattering, *Biochemistry 33*, 5531−5538.

BI051601B